European Conference on Computational Fluid Dynamics
ECCOMAS CFD 2006
P. Wesseling, E. Oñate and J. Périaux (Eds)

DIRECT NUMERICAL SIMULATION OF THE INTERACTION BETWEEN UNSHEARED TURBULENCE AND A FREE-SLIP SURFACE

Gaelle Campagne*, Jean-Bernard Cazalbou, Laurent Joly and Patrick Chassaing†

*ENSICA, Département de Mécanique des Fluides
1 place Emile Blouin, 31056 Toulouse, France
e-mail: gaelle.campagne@ensica.fr
† also at INPT-ENSEEIHT-IMFT UMR 5502 CNRS

Key words: Turbulence, Direct numerical simulation, Free surface, Random forcing

Abstract. *In this paper, direct numerical simulation is used to study the interaction between turbulence and a free surface. The configuration is original due to the fact that a random force generates turbulence in the vicinity of a plane parallel to the free surface. Turbulence is therefore statistically steady and nearly isotropic at some distance of the surface. A detailed description of the flow is provided, including second-order statistics and full Reynolds-stress budgets. It is shown that the results obtained in this configuration can help the understanding of intercomponent energy-transfer mechanisms.*

1 INTRODUCTION

Turbulence interacting with a free-slip surface is encountered in many flows of engineering interest. The most obvious are those of a liquid near a gas-liquid interface like, for instance, the surface layer of the ocean and lakes, stirred fluids within vessels, and many flows which occur in chemical engineering processes. On another hand, it can be viewed as a first approach to the physics of near-wall turbulence since it helps to evaluate the effects of kinematic blocking independently of the viscous effects, and of those effects induced by the almost systematic presence of mean shear in the vicinity of a solid wall. Kinematic blocking is known to affect the mechanism of intercomponent energy transfer (embodied in the Reynolds-stress-transport equations through the pressure-strain correlations): In an unbounded turbulent flow, at moderate levels of anisotropy, the mechanism of the intercomponent energy transfer can be viewed as a simple return-to-isotropy phenomenon. The picture changes drastically in the immediate vicinity of a blocking surface where, whatever the anisotropy, energy transfer is always at the expense of the normal component of the fluctuations. Such a modification has long been attributed to the so-called splat effect: blobs of fluid moving toward the surface transfer energy from the normal to

the tangential directions at the impact. This simple phenomenology has been questioned by Perot and Moin[1] who noticed that splat events should necessarily be balanced by "anti-splat" events with an opposite effect on the energy transfer. As a result, they suggested that the imbalance is small —hence the pressure-strain correlation— and can only be determined by viscous effects along the surface. This was supported by their direct numerical simulation of decaying turbulence near a free surface at short times. In another simulation of the same flow at larger times, Walker *et al.*[2] came to a slightly different conclusion: According to them, the imbalance between splat and anti-splat events results from conflicting contributions from the kinematic blocking and the return-to-isotropy mechanism which is present at large times (when anisotropy due to the presence of the surface becomes significant.) The results based on rapid distortion theory obtained by Magnaudet[3] confirm this last statement, and highlight the fact that the intercomponent energy transfer mechanism in the presence of a blocking surface strongly depends on the nature of turbulence at a distance: whether it is steady or unsteady, isotropic or not, etc.

The present study aims at complementing our view of these transfer phenomena when turbulence at a distance remains steady and quasi-isotropic. We believe that this case is more representative of engineering applications for which turbulence-production regions are present in the flow field, and continuously feed the surface regions via turbulent transport. To this end, we have defined a numerical analog of the oscillating-grid experiments (see, for instance De Silva and Fernando[4]). This configuration is characterized by statistical steadiness and continuous feeding of the surface by turbulent diffusion from a turbulence-production layer. It bears some similarities with the free-surface of an open-channel flow (see, for instance, the numerical simulations of Handler *et al.*[5]), but ensures strictly-zero mean shear in the surface region and, from a computational point of view, maximizes the number of grid points placed there. The final goal of our study will be to identify the structures responsible for the modifications induced by the presence of a free surface to the intercomponent energy transfer, and to give some informations about a physically-consistent formulation of a statistical model for the pressure-strain correlations.

The paper is organized as follows: Details about the computational method and the configuration are given in section 2. A description of the flow based on the examination of the second-order statistics is then provided in section 3, while section 4 is devoted to the presentation of the Reynolds-stress budgets. General comments and direction for future work are provided as the conclusion.

2 CALCULATION METHOD AND DEFINITION OF THE FLOW CASE

Our results are obtained from a numerical solution of the three-dimensional time-dependent Navier-Stokes equations. We discuss the computational method with a particular attention to the forcing technique —how turbulence is generated— and then, describe the way statistics are obtained. All the parameters of the solution are then given, together with a description of its specific features.

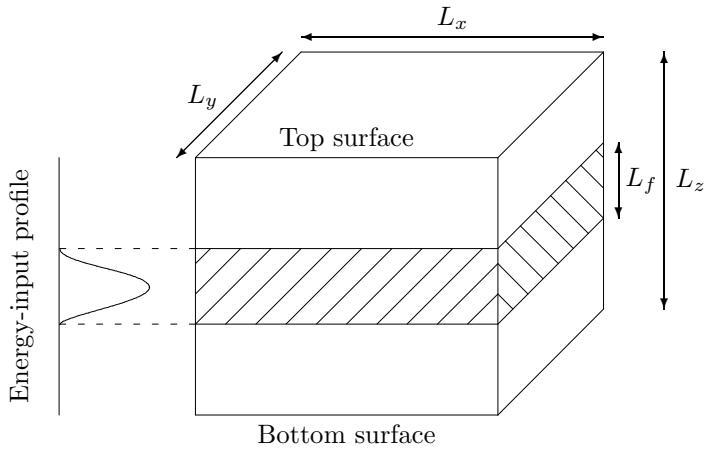

L_x	2π
L_y	2π
L_z	$7\pi/4$
L_f	$7\pi/12$

Figure 1: Definition of the computational domain. Turbulence production is strictly zero outside of the forcing region.

2.1 Computational method

As one can see in figure 1, the computational domain is a rectangular box in which the grid spacing is equal and uniform in each direction. The two horizontal directions, x and y, are periodical, with a period of 2π. The wave numbers are made nondimensional with $L_x = 2\pi$, and all the resolved wave numbers κ are therefore integer numbers. Symmetry conditions are imposed in the z direction to force free-surface boundary conditions. A random volume force, confined in the vicinity of a central plane parallel to the free surfaces, represents the steady source of turbulence.

The incompressible Navier-Stokes equations are solved under the form

$$\left\{ \begin{array}{ll} \boldsymbol{\nabla .}\ \boldsymbol{u} & = 0 \\ \partial_t\ \boldsymbol{u} & = \boldsymbol{u} \times (\boldsymbol{\nabla} \times \boldsymbol{u}) - \boldsymbol{\nabla}\ (P/\rho + \boldsymbol{u}^2/2) + \nu\ \boldsymbol{\Delta}\ \boldsymbol{u} \end{array} \right. \tag{1}$$

using a pseudo-spectral method, similar to that of Orszag and Patterson.[6] The momentum equation is advanced in time using a third-order Runge-Kutta scheme with implicit treatment of the diffusive term. Unlike the periodic x and y directions, odd and even symmetries along the z direction deserve a specific treatment. The (even) tangential velocities and (odd) normal velocity are decomposed using cosine and sine transforms, respectively. Such a procedure enforces the impermeability and free-slip boundary conditions at the top and bottom surfaces:

$$w|_{z=0} = w|_{z=2\pi} = 0, \quad \left.\frac{\partial u}{\partial z}\right|_{z=0} = \left.\frac{\partial u}{\partial z}\right|_{z=2\pi} = 0 \quad \text{and} \quad \left.\frac{\partial v}{\partial z}\right|_{z=0} = \left.\frac{\partial v}{\partial z}\right|_{z=2\pi} = 0.$$

Forcing method Among the available methods for the numerical generation of statistically steady turbulent flows, we have followed the method of Alvelius.[7] A fully random

three-dimensional force field is generated in the whole computational domain. It is implemented in spectral space and concentrated at small wave numbers according to a given spectrum $E(\kappa) \propto \exp[-(\kappa - \kappa_f)^2/c]$. We choose the forcing wave number $\kappa_f = 4$ and a concentration parameter $c = 0.05$, the result of which is to confine the input of energy in the range $\kappa = 2$ to $\kappa = 6$. By construction, the random force is divergence free so that it does not influence the pressure field. Confinement of the forcing in the vicinity of a central plane parallel to the free surfaces is performed using a Heaviside function modulated by a sine function (see figure 1). The energy density injected by the forcing function at each time step is then equal to $P = 0.025$. After a transient stage needed for the dissipation to adapt to the amount of energy-power input, turbulence reaches a statistically steady state.

Calculation of the statistics Calculation of the statistics benefits from several properties of the solution: (i) statistical homogeneity in planes parallel to the surfaces, (ii) invariance under reflection about the midplane, (iii) invariance under rotation about the z axis, and (iv) statistical steadiness. For a given time, statistical quantities are calculated by first averaging over planes parallel to the free surface. Symmetry about the midplane is then used to average the data between planes located at an equal distance from each of the free surfaces. Finally, rotational invariance about z is used to average correlations involving tangential components of the fluctuation. The results of this spatial averaging phase are further averaged in time with samples spaced by half the large eddy turnover time τ. Hence, for a calculation performed on a $n_x \times n_y \times n_z$ domain during a time interval equal to $n_\tau \times \tau$, the z-dependent statistics rely on $2n_x n_y n_\tau$ samples for correlations involving w, and twice that number for those involving at least one of the tangential velocity components. In the case presented below, we have:

$$n_x = n_y = 192, \quad n_z = 168 \quad \text{and} \quad n_\tau = 498.$$

2.2 Parameters and general properties of the solution

Definition of the computed flow Given the general dimensions and discretization of the computational domain, the flow will be fully defined by the value of the viscosity (ν). This value must be selected according to a resolution criterion for the smallest scales ($\kappa_{\max}$). We use $\kappa_{\max}\eta = 1.5$ (η is the Kolmogorov lengthscale), and $\kappa_{\max}$ is taken as $n_x/3$ in order to avoid antialiasing in agreement with the two-third rule. Analysis of the result in the next sections will need meaningful references, we can use several sets of characteristic scales,

- surface references: the values k_s and ϵ_s of the turbulent kinetic energy and dissipation rate at the surface, the corresponding turbulent Reynolds number Re_s is defined as $k_s^2/(\nu\epsilon_s)$;
- forcing references: the values k_f and ϵ_f at the edge of the forcing region and $Re_f = k_f^2/(\nu\epsilon_f)$.

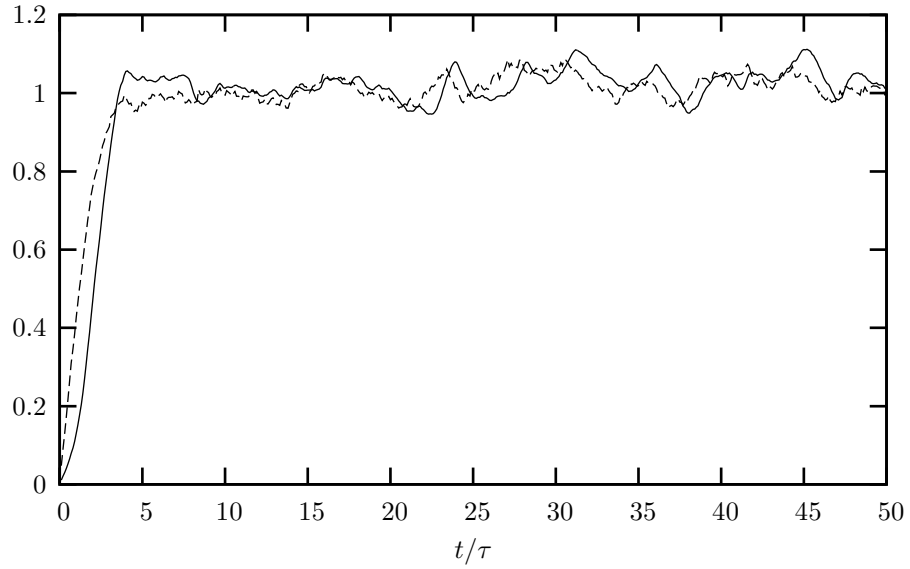

Figure 2: Time evolutions of the volume-averaged turbulent kinetic energy (– –) and dissipation rate (—), normalized by their final volume averages.

Quantities made nondimensional with the surface characteristic scales will be denoted by a star as a superscript, and those using the forcing scales by a tilde. Table 1 below gives the characteristics of the computed flow according to these two sets of references.

Re_s	z_f^*	Re_f	$\tilde{z}_f$	ν
76.5	1.20	132.5	2.33	2.0 10^{-3}

Table 1: Definition of the flow case. The distance between the bottom surface and the edge of the forcing region is denoted as $z_f = (L_z - L_f)/2$ and is given in both surface and forcing references.

Establishment of the fluctuating field Figure 2 shows the time evolutions of the volume-averaged turbulent kinetic energy $\langle k \rangle$ and dissipation rate $\langle \epsilon \rangle$ normalized by their final steady-state values (angle brackets denote volume average at a given time). The initial field is at rest when the forcing is switched on. Turbulence initiated in the forcing region is then diffused in the whole domain. After a transient stage equal to approximately 5 characteristic timescales, the flow reaches a statistical steady state: the figure shows that the volume averages of the turbulent kinetic energy and dissipation rate rise up to significant levels and fluctuate around these (constant) levels. In our study, turbulence production does not rely on the existence of mean-velocity gradients. The absence of a mean flow can be checked in figure 3 where the time evolutions of the volume-averaged components of the velocity field normalized by their r.m.s. final values have been plotted. One can see that these averages are less than 0.15 % at any time. The energy-spectrum

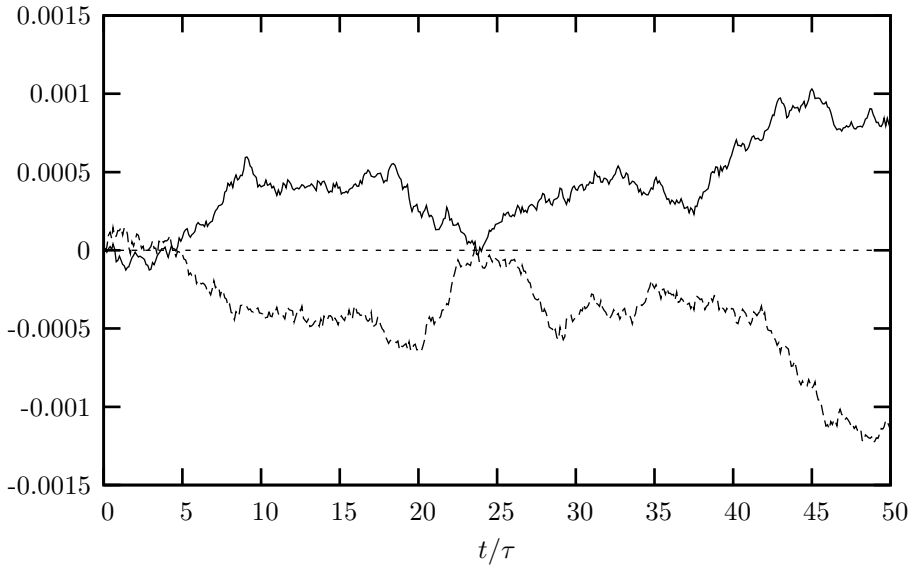

Figure 3: Time evolution of the volume average of each of the three components of the velocity field, normalized by their root-mean-square final values: $\langle U \rangle$ (—), $\langle V \rangle$ (– –), $\langle W \rangle$ (···).

function obtained at steady state in the domain is plotted in figure 4, it presents several characteristics worth to mention. First, the input of energy at $\kappa = 4$ is clearly visible on the plot. With increasing wave numbers, a region of limited extension exhibiting the Kolmogorov $-5/3$ slope follows, before the dissipation cut-off. At the high end of the spectrum, a slight pile-up of kinetic energy results from a good compromise between the value reached by the Reynolds number and the resolution of the smallest scales. This pile-up can be reduced by increasing the resolution criterion, but we have checked in a grid-independence study that the main part of the spectrum was unaffected as soon as $\kappa_{\max}\eta = 1.5$.

3 SECOND-ORDER STATISTICS

Figure 5 shows the profiles of the turbulent kinetic energy and Reynolds stresses, made nondimensional by k_s. The top of the figure corresponds to the lower edge of the forcing region. The maximum of each of these three quantities is located there. Then, they decrease toward the bottom surface. As the surface is approached, the normal Reynolds stress ($\overline{w^2}$) is forced to zero by the impermeability condition, while the tangential Reynolds stress ($\overline{u^2}$) increases significantly to reach a local maximum at the surface. Intercomponent energy transfer probably contributes to this local maximum, but the turbulent kinetic energy profile also shows such a maximum at the surface, this latter effect cannot be explained by intercomponent energy transfer. The simulations of Perot and Moin[1] and Walker *et al.*[2] for an ideal free surface also showed such a peak, in both studies it was suggested that the peak was due to a decrease in the dissipation rate. Our Reynolds-stress

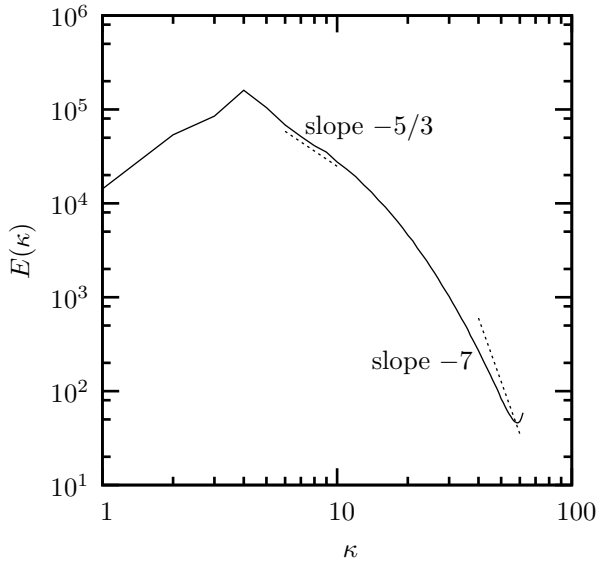

Figure 4: Energy-spectrum function at $t^* = 50$.

budgets presented in section 4 will support this interpretation.

The difference in the behaviour of the two Reynolds stresses is evidenced by the evolution of the isotropy factor defined as $I = w'/u'$, where u' and w' are the r.m.s. values of the tangential and horizontal components of the fluctuation. Figure 6 presents the vertical profile of this quantity. In the middle of the production region z_c, turbulence is slightly anisotropic ($I \approx 0.9$) at the expense of the vertical component of the fluctuation. As the random force field is isotropic, this is probably due to the z-confinement of the forcing. At the lower edge of the production region and moving toward the surface, the isotropy factor starts to increase to reach a maximum value about 1.16 at $z_s^* = 0.79$. At this location, w' is therefore higher than u' which is consistent with the experiments of turbulent diffusion from a plane source (oscillating-grid experiments, see De Silva and Fernando[4] for instance) where the isotropy factor is in the range 1.1–1.3. After reaching this maximum, the isotropy factor goes to zero at the free surface. We shall consider that the region located between the surface and z_s is the surface-influenced region and call it the *surface layer*.

We present in figure 7(a,b) the evolutions of different lengthscales: the turbulence lengthscale $\ell = k^{3/2}/\epsilon$, the longitudinal and transverse microscales λ_f and λ_g. The longitudinal microscale $\lambda_f = \lambda_x^u$ is associated to gradients of tangential velocities and the transverse microscale $\lambda_g = \lambda_x^w$ to the gradients of normal velocities. Between the lower edge of the forcing region and the top of the surface region, the turbulent lengthscale and the microscales exhibit different behaviours, the former slightly decreases while the latters increase. In this region, the two microscales remain approximately proportional, their ratio being about 1.30 is slightly lower than $\sqrt{2}$ (the value obtained in isotropic turbulence). In purely-diffusive turbulence, all lengthscales should increase with the distance from the

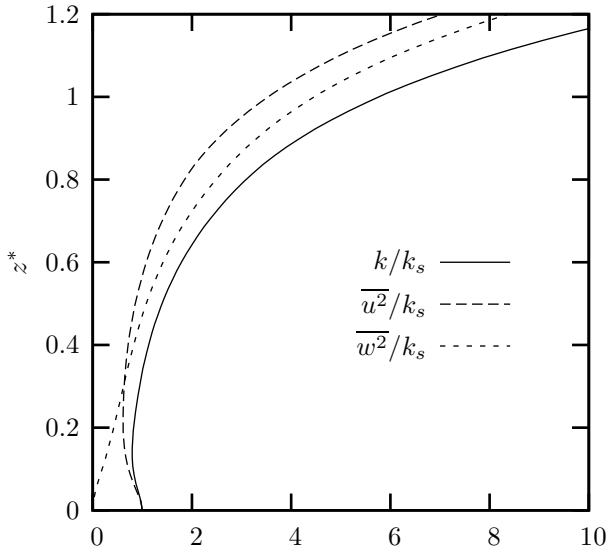

Figure 5: Profiles of the turbulent kinetic energy and Reynolds stresses across the zero-production region.

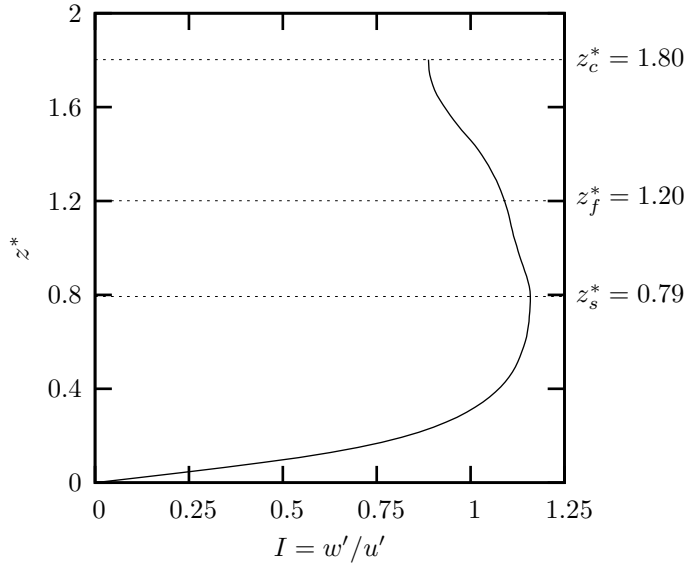

Figure 6: Vertical evolution of the isotropy factor. The dotted lines at $z = z_c$, $z = z_f$ and $z = z_s$ indicate, respectively, the midplane, lower edge of the production region and top of the surface layer.(All data are normalized with surface references.)

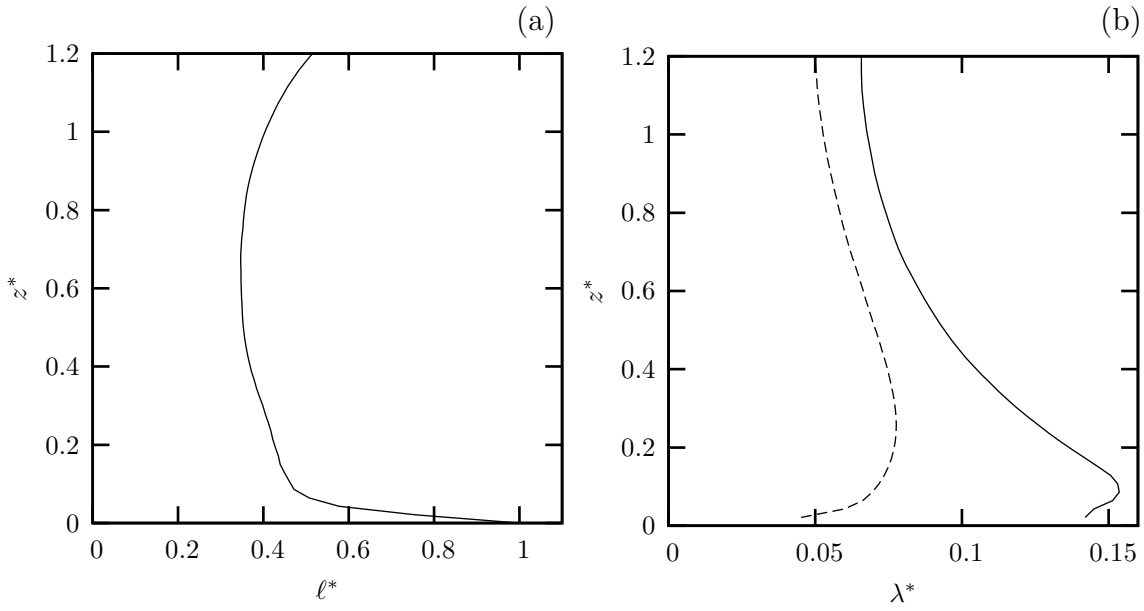

Figure 7: (a) Profile of the turbulent lengthscale ℓ^*. (b) Profiles of the Taylor microscales λ_f^* (—) and λ_g^* (– –). (All data are normalized with surface references.)

source. However, such behaviour relies on a self-similarity hypothesis which is obviously not satisfied here due to the limited size of the pure-diffusion region. That is probably the reason why ℓ decreases there. In the surface region, the evolution of the different lengthscales exhibit some similarities. All of them steadily increase as the surface is approached except very near the surface where they experience a rapid change: ℓ exhibits a sharp peak and the microscales decrease. This region of abrupt change should correspond to what is usually called *the viscous layer* (see Magnaudet[3]). We can estimate the height z_v of this viscous layer with the location of the maximum of λ_f, and retain $z_v^* \approx 0.09$.

The evolutions of the Reynolds numbers based on the turbulent lengthscale and microscales across the flow are plotted in figure 8(a,b). The Reynolds numbers based on the microscales are defined by $Re_\lambda = \lambda\sqrt{1.5k}/\nu$. All three Reynolds numbers decrease consistently across the pure-diffusion region. In the surface layer, their evolutions share the characteristics of those of the lengthscales: a mild variation across most of the layer followed by rapid changes in the viscous-layer. At this point, we note that the Reynolds numbers are not small in the so-called viscous layer: the turbulence Reynolds number and the longitudinal microscale Reynolds number rise up to values which are comparable to those obtained at the top of the surface layer. Examination of the Reynolds-stress budgets in the next section will also show that turbulent diffusion is not small as compared to viscous diffusion in this region, the term "viscous layer" will be kept in the following but should therefore be used with caution.

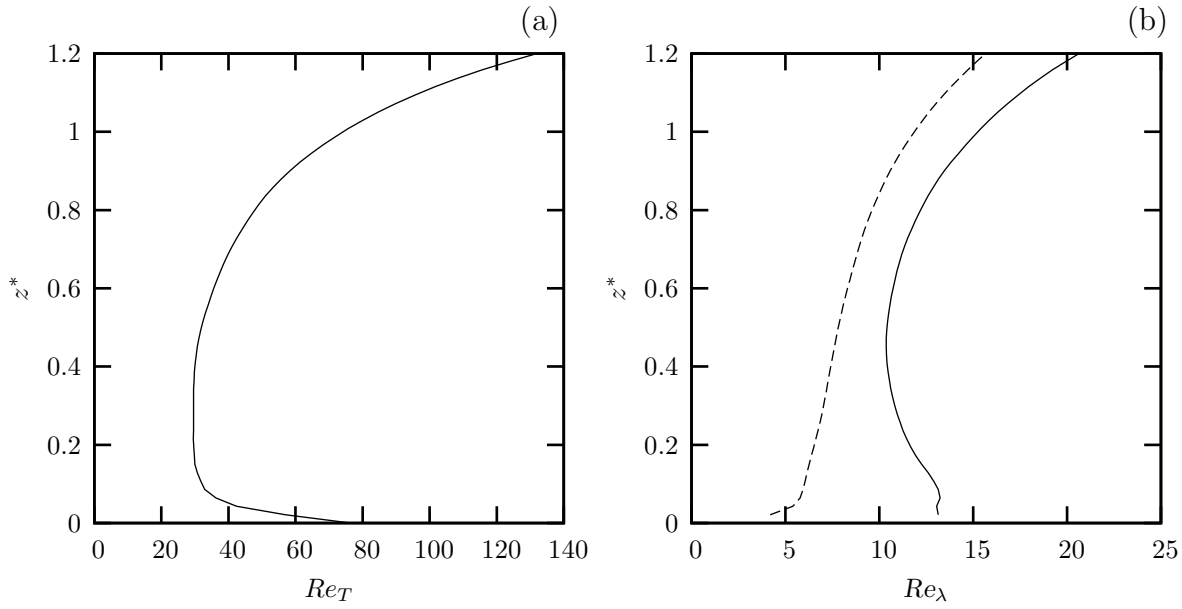

Figure 8: (a) Profile of the turbulent Reynolds number based on the turbulent lengthscale ℓ. (b) Profiles of the Reynolds numbers based on the longitudinal and transverse Taylor microscales λ_f (—) and λ_g (– –). At the top of the surface layer ($z = z_s$), we have $Re_T = 48$ and $Re_{\lambda f} = 13$ and, at the surface (z=0), $Re_T = 76$ and $Re_{\lambda f} = 13$.

4 REYNOLDS-STRESS BUDGETS

Transport equations for the components of the Reynolds-stress tensor $\overline{u_i u_j}$ are easily derived from the incompressible Navier-Stokes equations. When the flow is statistically steady with zero mean, they take the form

$$0 = \underbrace{-\frac{\partial \overline{u_i u_j u_k}}{\partial x_k}}_{\mathcal{D}^u_{ij}} \underbrace{-\frac{1}{\rho}\left(\frac{\partial \overline{p u_i}}{\partial x_j} + \frac{\partial \overline{p u_j}}{\partial x_i}\right)}_{\mathcal{D}^p_{ij}} + \underbrace{\nu \frac{\partial^2 \overline{u_i u_j}}{\partial x_k \partial x_k}}_{\mathcal{D}^\nu_{ij}} + \underbrace{\overline{\frac{p}{\rho}\left(\frac{\partial u_i}{\partial x_j} + \frac{\partial u_j}{\partial x_i}\right)}}_{\Pi_{ij}} \underbrace{- 2\nu \overline{\frac{\partial u_i}{\partial x_k}\frac{\partial u_j}{\partial x_k}}}_{\epsilon_{ij}}, \quad (2)$$

where $\mathcal{D}^u_{ij}$, $\mathcal{D}^p_{ij}$ and $\mathcal{D}^\nu_{ij}$ represent, respectively, diffusion by velocity fluctuations, pressure diffusion and viscosity; Π_{ij} represents the pressure-strain correlation and ϵ_{ij} the dissipation-rate tensor. These equations are valid outside of the forcing region, otherwise a production term corresponding to the random force would have to be added at the right hand side. Considering the symmetries of our problem, only $\overline{u^2}$ ($\equiv \overline{v^2}$) and $\overline{w^2}$ are nonzero among the components of the Reynolds-stress tensor, their transport equations take the form

$$0 = -\frac{\partial \overline{u^2 w}}{\partial z} + \nu \frac{\partial^2 \overline{u^2}}{\partial z^2} + 2\overline{\frac{p}{\rho}\frac{\partial u}{\partial x}} - 2\nu \overline{\frac{\partial u}{\partial x_k}\frac{\partial u}{\partial x_k}}, \quad (3)$$

$$0 = -\frac{\partial \overline{w^3}}{\partial z} - 2\frac{\partial}{\partial z}\left(\overline{\frac{p}{\rho} w}\right) + \nu \frac{\partial^2 \overline{w^2}}{\partial z^2} + 2\overline{\frac{p}{\rho}\frac{\partial w}{\partial z}} - 2\nu \overline{\frac{\partial w}{\partial x_k}\frac{\partial w}{\partial x_k}}. \quad (4)$$

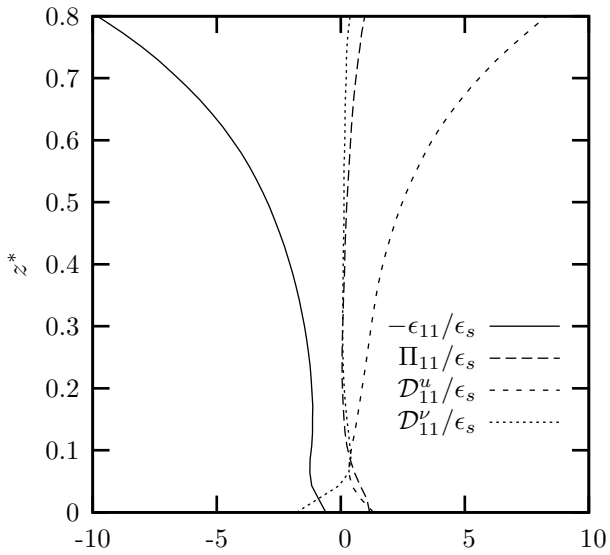

Figure 9: Tangential-stress ($\overline{u^2}$) budget plotted across the surface layer. (All data are normalized with surface references.)

As $k = \overline{u_i u_i}/2$, its transport equation can be deduced from the above:

$$0 = \underbrace{\underbrace{-\frac{1}{2}\frac{\partial\,\overline{u_i u_i w}}{\partial z}}_{\mathcal{D}^u} \underbrace{-\frac{\partial}{\partial z}\left(\overline{\frac{p}{\rho}\,w}\right)}_{\mathcal{D}^p}}_{\mathcal{D}^t} + \underbrace{\nu\,\frac{\partial^2\,\overline{k}}{\partial z^2}}_{\mathcal{D}^\nu} \underbrace{-\,\nu\,\overline{\frac{\partial u_i}{\partial x_k}\frac{\partial u_i}{\partial x_k}}}_{\epsilon}. \tag{5}$$

All the terms in equations (3–5) can be computed from the simulation results. The detailed structure of the budgets will be presented in the next paragraphs.

4.1 Tangential-stress budget

The budget of $\overline{u^2}$ across the surface layer is presented in figure 9. In the pure-diffusion region (between z_s and z_f) it closely resembles to that observed at the top of the surface layer and is therefore not reproduced here. At this location, the two dominant terms are the loss due to dissipation and the gain due to turbulent transport from the forcing region (by the velocity fluctuations only, since pressure diffusion is zero in this equation). A slight but noticeable positive contribution to the budget is also provided by the pressure-strain correlation. Recalling that the flow is slightly anisotropic in this region ($w' \approx 1.15u'$), it appears that the pressure-strain term acts conventionally as a return-to-isotropy term. As the surface is approached, dissipation and turbulent transport remain the dominant terms while the pressure-strain term goes to zero at $z^* \approx 0.3$, note that this is precisely the location where the isotropy factor reaches unity. The return-to-isotropy character of the intercomponent-energy-transfer process is thus remarkably verified down to this location.

Things really change in the viscous layer: all the terms in the budget become of the same order of magnitude. The viscous processes (diffusion and dissipation) both contribute negatively to the budget, they are balanced by the turbulent transport and pressure-strain terms. This exact balance between viscous and nonviscous terms confirms that the "viscous layer" is not fully dominated by viscosity and that such denomination may be misleading under certain circumstances. The value of the pressure-strain term clearly shows that intercomponent energy transfer is significant there, and acts in such a way that anisotropy is increased. Referring to the splat/anti-splat phenomenology introduced by Perot and Moin,[1] this would mean that the balance between splats and anti-splats is clearly in favour of the formers. A noticeable feature in the evolution of the dissipation rate in this region is the fact that, after reaching a moderate local maximum at the edge of the viscous layer ($\epsilon_{11} \approx 1.2\epsilon_s$), it decreases down to half this maximum at the surface ($\approx 0.6\epsilon_s$). This result is in agreement with the observations of Perot and Moin[1] and Walker *et al.*,[2] and supports the suggestion of these authors that such effect contributes to the increase of $\overline{u^2}$ at the surface. Note, however, that the value at the surface of the other contributor, the pressure-strain term, is nearly twice the "dissipation deficit" ($\Pi_{11} = 1.16\epsilon_s$). One last point worth to mention is the fact that, within the viscous layer, turbulent transport is antidiffusive. At present we are unable to provide an explanation of this result except that the counter-gradient character of diffusion by velocity fluctuations follows from Prandtl phenomenology which cannot be invoked when the characteristic scales of the fluctuating motion become of the same order as the distance to the blocking surface.

4.2 Normal-stress budget

Figure 10 shows the budget of $\overline{w^2}$ across the surface layer. As compared to the $\overline{u^2}$ budget, it involves one more term: pressure diffusion. The addition of this term and diffusion by velocity fluctuations will be denoted as the turbulent-transport term. At the top of the surface layer and down to $z^* \approx 0.3$, the budget shares the same characteristics as that of the tangential Reynolds stress: (i) it is dominated by turbulent transport from the forcing region and dissipation, (ii) the imbalance is accounted for by the pressure-strain correlation that acts as a return-to-isotropy term. We can notice, however, that turbulent diffusion by velocity fluctuations reaches much higher values than the corresponding term in the $\overline{u^2}$ budget. This is also true, although to a lesser extend, when turbulent transport as a whole is considered, and should explain why the isotropy factor is above unity in this region. Note also that pressure diffusion is antidiffusive, as usually recognized for this term (see the model of Lumley[8]).

In the viscous layer, all the terms contribute significantly to the balance except very near the surface where diffusion by velocity fluctuations goes to zero. In this region, the dissipation and the pressure-strain correlation both contribute negatively to the budget, the latter acting — as expected — against a return to isotropy. The positive contributions to the budget come from pressure diffusion and viscous diffusion. Nonviscous contributions

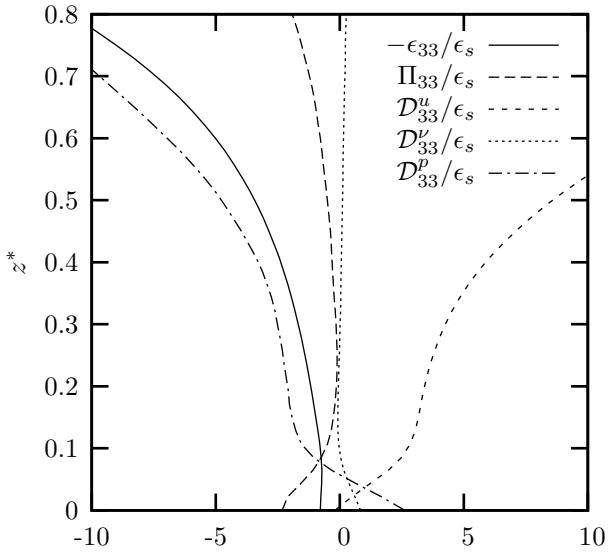

Figure 10: Normal-stress ($\overline{w^2}$) budget plotted across the surface layer. (All data are normalized with surface references.)

($\mathcal{D}^p_{33}$ and Π_{33}) are equal in magnitude and significantly higher ($\times 3$ at the surface) than the viscous contributions (ϵ_{33} and $\mathcal{D}^u_{33}$) which are also equal in magnitude. Another characteristic of the budget in this region is that pressure diffusion, which is antidiffusive in the top of the surface layer, now becomes diffusive. As mentioned above, this is at odds with the usual behaviour of this term.

4.3 Turbulent-kinetic-energy budget

In the turbulent-kinetic-energy budget, plotted in figure 11, we have regrouped turbulent transport in a single term. Consistently with the previously presented budgets, the level of turbulent kinetic energy level in the top of the surface region mainly results from turbulent transport from the forcing region and dissipation, viscous diffusion being negligible. In the viscous region, viscous diffusion and dissipation are comparable and contribute negatively to the budget, they are balanced by turbulent transport which is about twice as large as each of the latters. As in the $\overline{u^2}$ budget, we can observe a dissipation deficit at the surface which is most probably one of the reasons for the increase of k there. Regrouping diffusion by velocity and pressure fluctuations in a single term helps to show that turbulent transport as a whole behaves as an antidiffusive process in the viscous layer. This unusual behaviour also contributes to the increase of the turbulent-kinetic-energy level at the surface.

5 SUMMARY AND CONCLUSION

The results presented in this paper shed some light on the interaction between turbulence and a free surface. Direct numerical simulation is performed in an original configura-

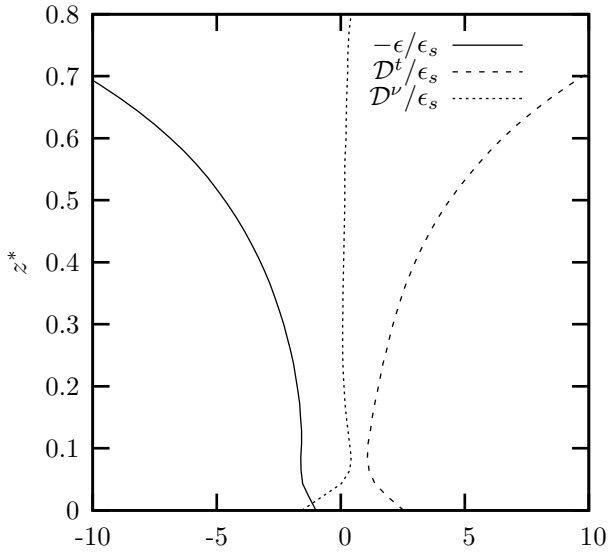

Figure 11: Turbulent-kinetic-energy budget plotted across the surface layer. (All data are normalized with surface references.)

tion where turbulence is continuously generated without mean shear in a finite-width layer parallel to the free surface. As a result the flow is statistically steady, turbulence remains nearly isotropic at some distance of the surface, and the surface layer is continuously fed by turbulent diffusion.

Examination of the statistics allows to identify a surface layer where the isotropy factor responds to the two-component limit imposed at the surface. Rapid changes in the profiles of the Reynolds stresses and characteristic lengthscales suggest the presence of a subregion located close to the surface within the surface layer. This region is usually called the viscous layer. Given the parameters of the simulation, both regions are easily distinguished, the surface layer being nearly ten times thicker than the viscous layer.

Inspection of the Reynolds-stress budget supports this partition of the flow: The upper part of the surface layer exhibits roughly the same kind of balance as that of a purely-diffusive turbulence, while the structure of the budgets radically changes in the viscous layer.

On the overall, three major conclusions can be drawn from our study:

- The pressure-strain correlation is an important term close to the wall, this makes our results closer to those obtained by Perot and Moin[1] in the simulation of decaying turbulence near a free surface at short times than to those of Walker *et al.*[2] in the same situation at large times. It supports the interpretation of Walker *et al.* according to which anisotropy, present at large time in their simulation, is responsible for a return-to-isotropy mechanism superposed onto the splat/anti-splat phenomenology. This mechanism alters the balance between the two kinds of events and results in a lower level of pressure-strain correlation at the surface. In our con-

figuration, anisotropy remains close to unity far from the surface, the pressure-strain correlation is therefore small outside of the viscous region, but constitutes a major contributor to the budget near the surface. We may thus suspect a clear imbalance between splats and anti-splats in favour of the formers.

- The so-called viscous layer is not dominated by viscous effects: the viscous terms are not dominant in the budget, and the turbulent Reynolds numbers based on the tangential velocity fluctuations or $\sqrt{k}$ are equal or even higher than those recorded at the top of the surface layer.

- The turbulent-diffusion terms present a rather unconventional behaviour in the viscous layer. Turbulent diffusion by velocity fluctuations is "antidiffusive" in the tangential Reynolds-stress budget, and pressure diffusion is "diffusive" in the normal Reynolds-stress budget. As a result, turbulent transport of turbulent kinetic energy taken as a whole is antidiffusive in the viscous layer. From a modelling point of view, it may be a delicate task to reproduce such a behaviour with a gradient diffusion scheme: it was shown by Cazalbou and Chassaing[9] that such a model would lead to severe realizability problems.

Future work on the data obtained here will aim at investigating in more details the elementary structures responsible for the intercomponent energy transfer. Questions remain on these structures, whether they are all of the generic types "splat" and "anti-splat", if there is some possibility to quantify them separately. Answers to these questions would help to understand the influence of the nature of the blocking surface (rigid or free-slip) on the level of pressure-strain correlation.

REFERENCES

[1] B. Perot and P. Moin. Shear-free turbulent boundary layers. part 1. Physical insights into near-wall turbulence. *J. Fluid Mech.*, 295:199–227, 1995.

[2] D. T. Walker, R. I. Leighton, and L. O. Garza-Rios. Shear-free turbulence near a flat free surface. *J. Fluid Mech.*, 320:19–51, 1996.

[3] J. Magnaudet. High-Reynolds-number turbulence in a shear-free boundary layer: revisiting the Hunt-Graham theory. *J. Fluid Mech.*, 484:167–196, 2003.

[4] I. P. D. De Silva and H. J. S. Fernando. Oscillating grids as a source of nearly isotropic turbulence. *Phys. Fluids*, 6(7):2455–2464, 1994.

[5] R. A. Handler, T. F. Swean Jr., R. I. Leighton, and J. D. Swearingen. Length scales and the energy balance for turbulence near a free surface. *AIAA J.*, 31(11):1998–2007, 1993.

[6] S. A. Orszag and G. S. Patterson. Numerical simulation of three-dimensional homogeneous isotropic turbulence. *Phys. Fluids Rev. Let.*, 28(2):76–79, 1972.

[7] K. Alvelius. Random forcing of three-dimensional homogeneous turbulence. *Phys. Fluids*, 11(7):1880–1889, 1999.

[8] J. L. Lumley. Computational modelling of turbulent flows. *Advances in Applied Mechanics*, 18:123–176, 1978.

[9] J.-B. Cazalbou and P. Chassaing. The structure of the solution obtained with reynolds-stress-transport models at the free-stream edges of turbulent flows. *Phys. Fluids*, 14(2):597–611, february 2002.